Progress In Electromagnetics Research B, Vol. 48, 151–173, 2013

INFLUENCE OF THE SPOT-SIZE AND CROSS-SECTION ON THE OUTPUT FIELDS AND POWER DENSITY ALONG THE STRAIGHT HOLLOW WAVEGUIDE

Zion Menachem* **and Saad Tapuchi**

Department of Electrical Engineering, Sami Shamoon College of Engineering, Israel

Abstract—This paper presents a rigorous approach for the propagation of electromagnetic (EM) fields along a straight hollow waveguide with a circular cross section. The objectives are to present the technique to calculate the dielectric profiles and their transverse derivatives in the inhomogeneous cross section of the cylindrical hollow waveguide, and to understand the influence of the spot-size and cross section on the output fields and output power density. The derivation is based on Maxwell's equations. The longitudinal components of the fields are developed into the Fourier-Bessel series. The transverse components of the fields are expressed as functions of the longitudinal components in the Laplace plane and are obtained by using the inverse Laplace transform by the residue method. The separation of variables is obtained by using the orthogonal-relations. These objectives contribute to the application of the model for the straight hollow waveguide.

1. INTRODUCTION

Various methods for the analysis of cylindrical hollow metallic or metallic with inner dielectric coating waveguide have been studied in the literature. A review of the hollow waveguide technology [1, 2] and a review of IR transmitting, hollow waveguides, fibers and integrated optics [3] were published. Hollow waveguides with both metallic and dielectric internal layers have been proposed to reduce the transmission losses. Hollow-core waveguides have two possibilities. The inner core materials have refractive indices greater than one (namely, leaky waveguides) or the inner wall material has a refractive index of less than

Received 20 November 2012, Accepted 10 January 2013, Scheduled 26 January 2013

* Corresponding author: Zion Menachem (zionm@post.tau.ac.il).

one. A hollow waveguide can be made, in principle, from any flexible or rigid tube (plastic, glass, metal, etc.) if its inner hollow surface (the core) is covered by a metallic layer and a dielectric overlayer. This layer structure enables us to transmit both the TE and TM polarization with low attenuation [4, 5].

Light propagation in a cylindrical waveguide has been proposed [6]. The propagation of guided optical waves in circular waveguides made of concentric layers of glass, aluminium, and vacuum were investigated. In this work, attenuation is associated with the imaginary part of the dielectric constant of aluminum. To understand light propagation in circular dielectric waveguides with finite metal cladding, three different waveguide structures have been discussed.

In the advance finite dimensional algebraic function approximation technique in eigenvalue problems of lossless metallic guides filled with anisotropic and inhomogeneous media, to exact analysis in infinite dimensions, properties of the linear operator in infinite dimensions corresponding to Maxwell's equations have been investigated [7].

The method of algebraic function approximation in eigenvalue problems of closed lossless waveguides has been illustrated by means of two examples [8]. Numerical computation results have been presented for two physical problems. First, a closed uniform cylindrical guide loaded with a concentric ferrite tube was investigated. Next, a closed uniform cylindrical guide loaded with a coaxial cylindrical isotropic dielectric rod was taken up.

A general method has been proposed to frequency domain analysis of longitudinally inhomogeneous waveguides [9]. In this method, the electric permittivity and also the transverse electric and magnetic fields were expanded in a Taylor's series. The field solutions were obtained after finding unknown coefficients of the series. The unknown coefficients of the series were obtained from some recursive relations. A general method has been proposed to analyze aperiodic or periodic longitudinally inhomogeneous waveguides [10]. In this method, the electric permittivity function was expanded in the Fourier series. First, the periodic longitudinally inhomogeneous waveguides were analyzed using the Fourier series expansion of the electric permittivity function to find their propagation constant and characteristic impedances.

A numerical technique has been proposed for the analysis of various hollow conducting waveguides [11]. The method is based on mathematically modelling of physical response of a system to excitation over a range of frequencies. This is a mathematical model of the physical measurements when the resonant frequencies of a system were determined by the amplitude of response to some excitation. The response amplitudes were then used to determine the resonant

frequencies.

The main objectives of this paper are to present the technique to calculate the dielectric profiles and their transverse derivatives in the inhomogeneous cross section of the straight hollow waveguide, and to understand the influence of the spot-size and cross section on the output fields and output power density. The derivation is based on Maxwell's equations. The longitudinal components of the fields are developed into the Fourier-Bessel series. The transverse components of the fields are expressed as functions of the longitudinal components in the Laplace plane and are obtained by using the inverse Laplace transform by the residue method. The separation of variables is obtained by using the orthogonal-relations. These objectives contribute to the application of the model for the straight hollow waveguide. The results of this model are applied to the study of cylindrical hollow waveguides that are suitable for transmitting infrared radiation, especially CO_2 laser radiation. In this paper we assume that the modes excited at the input of the waveguide by the conventional CO_2 laser infrared (IR) radiation ($\lambda = 10.6\,\mu\text{m}$) are closer to the *TEM* polarization of the laser radiation. The TEM_{00} mode is the fundamental and the most important mode. This means that a cross-section of the beam has a Gaussian intensity distribution.

2. THE DERIVATION

The wave equations for the electric and magnetic field components in the inhomogeneous dielectric medium $\epsilon(r)$ are given for a lossy dielectric media in metallic boundaries of the waveguide. The cross-section of the straight hollow waveguide is shown in Fig. 1 for the application of the hollow waveguide, in the region $0 \leq r \leq a + \delta_m$, where δ_m is the thickness of the metallic layer, and d is the thickness of the dielectric layer.

The following derivation is given for the lossless case to simplify the mathematical expressions. In a linear lossy medium, the solution

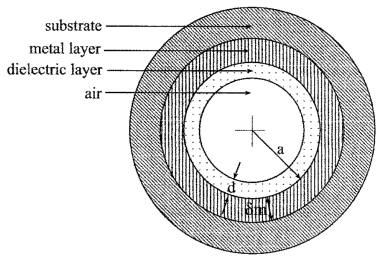

Figure 1. A cross-section of the straight hollow waveguide (r, θ).

is obtained by replacing the permittivity ϵ by $\epsilon_c = \epsilon - j(\sigma/\omega)$ in the solutions for the lossless case, where ϵ_c is the complex dielectric constant, and σ is the conductivity of the medium. The boundary conditions for a lossy medium are given after the derivation. For most materials, the permeability μ is equal to that of free space ($\mu = \mu_0$). The wave equations for the electric and magnetic field components in the inhomogeneous dielectric medium $\epsilon(r)$ are given by

$$\nabla^2\mathbf{E} + \omega^2\mu\epsilon\mathbf{E} + \nabla\left(\mathbf{E}\cdot\frac{\nabla\epsilon}{\epsilon}\right) = 0, \tag{1a}$$

and

$$\nabla^2\mathbf{H} + \omega^2\mu\epsilon\mathbf{H} + \frac{\nabla\epsilon}{\epsilon}\times(\nabla\times\mathbf{H}) = 0, \tag{1b}$$

respectively. The transverse dielectric profile is defined as $\epsilon(r) = \epsilon_0[1+g(r)]$, where ϵ_0 represents the vacuum dielectric constant, and $g(r)$ is its profile function in the waveguide. The normalized transverse derivative of the dielectric profile is defined as $g_r(r) = [1/\epsilon(r)][\partial\epsilon(r)/\partial r]$.

The z component of the exact Laplacian is given by

$$\left(\nabla^2\mathbf{E}\right)_z = \nabla^2 E_z = \frac{\partial^2}{\partial r^2}E_z + \frac{1}{r^2}\frac{\partial^2}{\partial\theta^2}E_z + \frac{1}{r}\frac{\partial}{\partial r}E_z + \frac{\partial^2}{\partial z^2}E_z. \tag{2}$$

The longitudinal components of the wave Eqs. (1a) and (1b) are taken into account, where

$$\left[\nabla\left(\mathbf{E}\cdot\frac{\nabla\epsilon}{\epsilon}\right)\right]_z = \frac{\partial}{\partial z}\left[E_r g_r\right], \tag{3}$$

and

$$\left[\frac{\nabla\epsilon}{\epsilon}\times(\nabla\times\mathbf{H})\right]_z = j\omega\epsilon\left[\frac{\nabla\epsilon}{\epsilon}\times\mathbf{E}\right]_z = j\omega\epsilon g_r E_\theta. \tag{4}$$

The longitudinal components of the wave Eqs. (1a) and (1b) are written in the form

$$\left(\nabla^2\mathbf{E}\right)_z + k^2 E_z + \frac{\partial}{\partial z}\left(E_r g_r\right) = 0, \tag{5}$$

$$\left(\nabla^2\mathbf{H}\right)_z + k^2 H_z + j\omega\epsilon g_r E_\theta = 0, \tag{6}$$

where $(\nabla^2\mathbf{E})_z$, for instance, is given according to (2). The *local* wave number parameter is $k = \omega\sqrt{\mu\epsilon(r)} = k_0\sqrt{1+g(r)}$, where the free-space wave number is $k_0 = \omega\sqrt{\mu_0\epsilon_0}$. The transverse Laplacian operator is defined as $\nabla_\perp^2 \equiv \nabla^2 - \partial^2/\partial z^2$.

The Laplace transform

$$\tilde{a}(s) = \mathcal{L}\{a(z)\} = \int_{z=0}^{\infty} a(z)e^{-sz}dz \tag{7}$$

is applied on the z-dimension, where $a(z)$ represents any z-dependent variables.

The longitudinal components of the fields are developed into Fourier-Bessel series, in order to satisfy the metallic boundary conditions of a circular cross-section. Suppose that we have only ideal boundary conditions for $r = a$. Thus, the electric and magnetic fields will be zero in the metal, $E_z(r = a) = 0$ and $[\partial/\partial r]H_z|_{r=a} = 0$. In addition, the Laplace transform will be zero in $r = a$. The longitudinal components of the fields (E_z, H_z) are developed into Fourier-Bessel series [12], as follows:

$$\tilde{E}_z(s) = \sum_{n'}\sum_{m'}\left[A_{n'm'}(s)\cos(n'\theta) + B_{n'm'}(s)\sin(n'\theta)\right]J_{n'}\left(P_{n'm'}\frac{r}{a}\right), \tag{8a}$$

$$\tilde{H}_z(s) = \sum_{n'}\sum_{m'}\left[C_{n'm'}(s)\cos(n'\theta) + D_{n'm'}(s)\sin(n'\theta)\right]J_{n'}\left(P'_{n'm'}\frac{r}{a}\right), \tag{8b}$$

where P_{nm} and P'_{nm} are the mth roots of the equations $J_n(x) = 0$ and $dJ_n(x)/dx = 0$, respectively.

By substituting Eq. (2) into Eq. (5) and by using the Laplace transform (7), the longitudinal components of the wave equations (Eqs. (5)–(6)) are described in the Laplace transform domain, as *coupled* wave equations, as follows:

$$\left(\nabla_\perp^2 + s^2 + k^2\right)\tilde{E}_z + sg_r\tilde{E}_r = g_rE_{r_0} + sE_{z_0} + E'_{z_0}, \tag{9a}$$

$$\left(\nabla_\perp^2 + s^2 + k^2\right)\tilde{H}_z + j\omega\epsilon g_r\tilde{E}_\theta = sH_{z_0} + H'_{z_0}, \tag{9b}$$

where E_{z0}, H_{z0}, E_{r_0}, E_{θ_0}, H_{r_0}, H_{θ_0} are the values of the corresponding fields at $z = 0$, i.e., $E_{z_0} = E_z(r, \theta, z = 0)$ and $E'_{z_0} = (\partial/\partial z)E_z(r, \theta, z)|_{z=0}$.

The transverse fields are obtained directly from the Maxwell equations, and by using the Laplace transform (7). The transverse fields of the straight hollow waveguide are dependent only on the longitudinal components of the fields, as follows:

$$\tilde{E}_r(s) = \frac{1}{s^2 + k^2}\left\{-\frac{j\omega\mu_0}{r}\frac{\partial}{\partial\theta}\tilde{H}_z + s\frac{\partial}{\partial r}\tilde{E}_z + sE_{r_0} - j\omega\mu_0H_{\theta_0}\right\}, \tag{10a}$$

$$\tilde{E}_\theta(s) = \frac{1}{s^2 + k^2}\left\{\frac{s}{r}\frac{\partial}{\partial\theta}\tilde{E}_z + j\omega\mu_0\frac{\partial}{\partial r}\tilde{H}_z + sE_{\theta_0} + j\omega\mu_0H_{r_0}\right\}, \tag{10b}$$

$$\tilde{H}_r(s) = \frac{1}{s^2+k^2}\left\{\frac{j\omega\epsilon}{r}\frac{\partial}{\partial\theta}\tilde{E}_z + s\frac{\partial}{\partial r}\tilde{H}_z + sH_{r_0} + j\omega\epsilon E_{\theta_0}\right\}, \quad (10c)$$

$$\tilde{H}_\theta(s) = \frac{1}{s^2+k^2}\left\{\frac{s}{r}\frac{\partial}{\partial\theta}\tilde{H}_z - j\omega\epsilon\frac{\partial}{\partial r}\tilde{E}_z + sH_{\theta_0} - j\omega\epsilon E_{r_0}\right\}, \quad (10d)$$

where z is the coordinate along the straight hollow waveguide.

The *coupled* wave Eqs. 9(a) and 9(b) become wave equations that are dependent only on the longitudinal components of the fields, by substituting the transverse fields (Eqs. 10(a)–10(d)) into the *coupled* wave equations (Eqs. 9(a) and 9(b)).

Two sets of equations are obtained by substitution the longitudinal components of the fields (Eqs. 8(a) and 8(b)) into the wave equations. The first set of the equations is multiplied by $\cos(n\theta)J_n(P_{nm}r/a)$, and after that by $\sin(n\theta)J_n(P_{nm}r/a)$, for $n \neq 0$. Similarly, the second set of the equations is multiplied by $\cos(n\theta)J_n(P'_{nm}r/a)$, and after that by $\sin(n\theta)J_n(P'_{nm}r/a)$, for $n \neq 0$. In order to find an algebraic system of four equations with four unknowns, it is necessary to integrate over the area (r,θ), where $r = [0,a]$, and $\theta = [0,2\pi]$, by using the orthogonal-relations $\int_0^{2\pi}\cos(n\theta)\cos(n'\theta)d\theta = \pi\delta_{nn'}$, $\int_0^{2\pi}\sin(n\theta)\sin(n'\theta)d\theta = \pi\delta_{nn'}$, and $\int_0^{2\pi}\sin(n\theta)\cos(n'\theta)d\theta = 0$, where $\delta_{nn'}$ is the Kronecker delta which equals unity for $n = n'$, and zero otherwise [13].

The propagation constants β_{nm} and β'_{nm} of the TM and TE modes of the hollow waveguide [14] are given, respectively, by $\beta_{nm} = \sqrt{k_o^2 - (P_{nm}/a)^2}$ and $\beta'_{nm} = \sqrt{k_o^2 - (P'_{nm}/a)^2}$, where the transverse Laplacian operator $(\nabla_\perp^2)$ is given by $-(P_{nm}/a)^2$ and $-(P'_{nm}/a)^2$ for the TM and TE modes of the hollow waveguide, respectively.

The separation of variables is obtained by using the preceding orthogonal-relations. Thus the algebraic equations $(n \neq 0)$ are given by

$$\alpha_n{}^{(1)}A_n + \beta_n{}^{(1)}D_n = \frac{1}{\pi}\left(\widehat{BC1}\right)_n, \quad (11a)$$

$$\alpha_n{}^{(2)}B_n + \beta_n{}^{(2)}C_n = \frac{1}{\pi}\left(\widehat{BC2}\right)_n, \quad (11b)$$

$$\beta_n{}^{(3)}B_n + \alpha_n{}^{(3)}C_n = \frac{1}{\pi}\left(\widehat{BC3}\right)_n, \quad (11c)$$

$$\beta_n{}^{(4)}A_n + \alpha_n{}^{(4)}D_n = \frac{1}{\pi}\left(\widehat{BC4}\right)_n. \quad (11d)$$

Further we assume $n' = n = 1$. The elements (${\alpha_n}^{(1)}$, ${\beta_n}^{(1)}$, etc), on the left side of (11a) for $n = 1$ are given by:

$$\begin{aligned}{\alpha_1}^{(1)mm'} = \pi\left(s^2+\beta_{1m'}^2\right)\left[\left(s^2+{k_0}^2\right)G_{00}^{(1)mm'}+{k_0}^2G_{01}^{(1)mm'}\right] \\ +\pi{k_0}^2\left(s^2G_{01}^{(1)mm'}+G_{02}^{(1)mm'}\right)+\pi s^2\left(G_{03}^{(1)mm'}\right), \quad (12a)\end{aligned}$$

$${\beta_1}^{(1)mm'} = -j\omega\mu_0\pi s\left(G_{04}^{(1)mm'}\right), \quad (12b)$$

where the elements of the matrices ($G_{00}^{(1)mm'}$, etc.) are given in Appendix A. Similarly, the other elements on the left side in Eqs. (11b)–(11d) are obtained. We establish an algebraic system of four equations with four unknowns. All the elements of the matrices in the Laplace transform domain are dependent on the Bessel-equations, the dielectric profile $g(r)$, the transverse derivative $g_r(r)$, the parameters of the cross-section (r, θ), and the propagation constants β_{nm} and β'_{nm} of the TM and TE modes of the hollow waveguide, respectively.

The elements of the boundary conditions' vectors on the right side in Eqs. (11a)–(11d) are changed at the entrance of the straight hollow waveguide, as follows:

$$\left(\widehat{BC1}\right)_1 = \int_0^{2\pi}\int_0^a (BC1)\cos(\theta)J_1(P_{1m}r/a)rdrd\theta, \quad (13a)$$

$$\left(\widehat{BC2}\right)_1 = \int_0^{2\pi}\int_0^a (BC2)\sin(\theta)J_1(P_{1m}r/a)rdrd\theta, \quad (13b)$$

$$\left(\widehat{BC3}\right)_1 = \int_0^{2\pi}\int_0^a (BC3)\cos(\theta)J_1(P'_{1m}r/a)rdrd\theta, \quad (13c)$$

$$\left(\widehat{BC4}\right)_1 = \int_0^{2\pi}\int_0^a (BC4)\sin(\theta)J_1(P'_{1m}r/a)rdrd\theta. \quad (13d)$$

In the case of the TEM_{00} mode in excitation for the straight hollow waveguide, the elements of the boundary conditions' vectors (Eqs. (13a)–(13d)) are obtained, where:

$$BC1 = BC2 = j\omega\mu_0 H^+_{\theta_0}sg_r + k^2E^+_{r_0}g_r, \quad (14a)$$

$$BC3 = BC4 = -j\omega\epsilon E^+_{\theta_0}sg_r + k^2H^+_{r_0}g_r. \quad (14b)$$

The elements of the boundary conditions (e.g., $(\widehat{BC2})_1$) at $z = 0^+$

according to Eq. (13b) is given where

$$(BC2) = \left[\left(s^2 + k^2\right)\left(sE_{z_0} + E'_{z_0}\right)\right] + j\omega\mu_0 H_{\theta_0} s g_r + k^2 E_{r_0} g_r.$$

The boundary conditions at $z = 0^+$ for TEM_{00} mode in excitation become to:

$$\left(\widehat{BC2}\right)_1 = 2\pi\left\{\int_0^a Q(r)(k(r) + js)k(r)J_{1m}(P_{1m}r/a)rdr\right\}\delta_{1n} \quad (15)$$

where

$$Q(r) = \frac{E_0}{n_c(r) + 1} g_r \exp\left(-(r/w_o)^2\right).$$

Similarly, the remaining elements of the boundary conditions at $z = 0^+$ are obtained. The matrix system of the Eqs. (11a)–(11d) is solved to obtain the coefficients (A_1, B_1, etc.).

According to the Gaussian beams [15] the parameter w_0 is the minimum spot-size at the plane $z = 0$ (see Fig. 2), and the electric field at the plane $z = 0$ is given by $E = E_0 \exp[-(r/w_o)^2]$. The modes excited at $z = 0$ in the waveguide by the conventional CO_2 laser IR radiation ($\lambda = 10.6\,\mu\text{m}$) are closer to the TEM polarization of the laser radiation. The TEM_{00} mode is the fundamental and the most important mode. This means that a cross-section of the beam has a Gaussian intensity distribution. The relation between the electric and magnetic fields [15] is given by $E/H = \sqrt{\mu_0/\epsilon_0} \equiv \eta_0$, where η_0 is the intrinsic wave impedance. Suppose that the electric field is parallel to the y-axis. Thus the components of E_y and H_x are written by the fields $E_y = E_0 \exp[-(r/w_o)^2]$ and $H_x = -(E_0/\eta_0)\exp[-(r/w_o)^2]$.

After a Gaussian beam passes through a lens and before it enters to the waveguide, the waist cross-sectional diameter ($2w_0$) can then be calculated approximately for a parallel incident beam by means of $w_0 = \lambda/(\pi\theta) \simeq (f\lambda)/(\pi w)$. This approximation is justified if the parameter w_0 is much larger than the wavelength λ. The asymptotic angle of the beam is a function of the laser beam cross-sectional

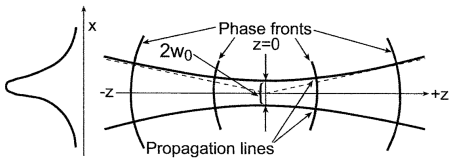

Figure 2. Propagating Gaussian beam.

diameter ($2w$) at the lens plane, and a function of the focal length of the lens f. The parameter of the waist cross-sectional diameter ($2w_0$) is taken into account in our method, instead of the focal length of the lens (f). The initial fields at $z = 0^+$ are formulated by using the Fresnel coefficients of the transmitted fields [16], as follows

$$E^+_{r_0}(r,\theta,z=0^+) = T_E(r)(E_0 e^{-(r/w_o)^2}\sin\theta), \tag{16a}$$

$$E^+_{\theta_0}(r,\theta,z=0^+) = T_E(r)\left(E_0 e^{-(r/w_o)^2}\cos\theta\right), \tag{16b}$$

$$H^+_{r_0}(r,\theta,z=0^+) = -T_H(r)\left((E_0/\eta_0) e^{-(r/w_o)^2}\cos\theta\right), \tag{16c}$$

$$H^+_{\theta_0}\left(r,\theta,z=0^+\right) = T_H(r)\left((E_0/\eta_0) e^{-(r/w_o)^2}\sin\theta\right), \tag{16d}$$

where $E^+_{z_0} = H^+_{z_0} = 0$, $T_E(r) = 2/[(n(r)+1]$, $T_H(r) = 2n(r)/[(n(r)+1]$, and $n(r) = [\epsilon_r(r)]^{1/2}$. The index of refraction is denoted by $n(r)$.

The output transverse components of the fields of the straight hollow waveguide are finally expressed in a form of *transfer matrix functions*, as follows:

$$\begin{aligned} E_r(r,\theta,z) = {} & E^+_{r0}e^{-jkz} + \frac{j\omega\mu_0}{r}\sin\theta\sum_{m'} C^{m'}_{S1}(z)J_1(\psi) \\ & -\frac{j\omega\mu_0}{r}\cos\theta\sum_{m'} D^{m'}_{S1}(z)J_1(\psi) + \cos\theta\sum_{m'} A^{m'}_{S2}(z)\frac{dJ_1}{dr}(\xi) \\ & +\sin\theta\sum_{m'} B^{m'}_{S2}(z)\frac{dJ_1}{dr}(\xi), \end{aligned} \tag{17a}$$

$$\begin{aligned} E_\theta(r,\theta,z) = {} & E^+_{\theta0}e^{-jkz} + j\omega\mu_0\cos\theta\sum_{m'} C^{m'}_{S1}(z)\frac{dJ_1}{dr}(\psi) \\ & +j\omega\mu_0\sin\theta\sum_{m'} D^{m'}_{S1}(z)\frac{dJ_1}{dr}(\psi) - \frac{1}{r}\sin\theta\sum_{m'} A^{m'}_{S2}(z)J_1(\xi) \\ & +\frac{1}{r}\cos\theta\sum_{m'} B^{m'}_{S2}(z)J_1(\xi), \end{aligned} \tag{17b}$$

$$\begin{aligned} H_r(r,\theta,z) = {} & H^+_{r0}e^{-jkz} - \frac{j\omega\epsilon}{r}\sin\theta\sum_{m'} A^{m'}_{S1}(z)J_1(\xi) \\ & +\frac{j\omega\epsilon}{r}\cos\theta\sum_{m'} B^{m'}_{S1}(z)J_1(\xi) + \cos\theta\sum_{m'} C^{m'}_{S2}(z)\frac{dJ_1}{dr}(\psi) \\ & +\cos\theta\sum_{m'} C^{m'}_{S2}(z)\frac{dJ_1}{dr}(\psi) + \sin\theta\sum_{m'} D^{m'}_{S2}(z)\frac{dJ_1}{dr}(\psi), \end{aligned} \tag{17c}$$

$$H_\theta(r,\theta,z) = H_{\theta 0}^{+} e^{-jkz} - j\omega\epsilon\cos\theta \sum_{m'} A_{S1}^{m'}(z)\frac{dJ_1}{dr}(\xi)$$
$$-j\omega\epsilon\sin\theta\sum_{m'} B_{S1}^{m'}(z)\frac{dJ_1}{dr}(\xi) - \frac{1}{r}\sin\theta\sum_{m'} C_{S2}^{m'}(z)J_1(\psi)$$
$$+\frac{1}{r}\cos\theta\sum_{m'} D_{S2}^{m'}(z)J_1(\psi), \tag{17d}$$

where $\psi = [P'_{1m'}(r/a)]$ and $\xi = [P_{1m'}(r/a)]$. The coefficients are given in the above equation, for instance

$$A_{S1}^{m'}(z) \;=\; \mathcal{L}^{-1}\left\{\frac{A_{1m'}(s)}{s^2+k^2(r)}\right\}, \tag{18a}$$

$$A_{S2}^{m'}(z) \;=\; \mathcal{L}^{-1}\left\{\frac{sA_{1m'}(s)}{s^2+k^2(r)}\right\}, \tag{18b}$$

where

$$m' = 1,\ldots,N, \quad 3 \le N \le 20. \tag{18c}$$

The roots (zeros) of the equations $J_1(x) = 0$ and $dJ_1(x)/dx = 0$ are given by the ready tables [17, 18].

The inverse Laplace transform is performed in this study by a direct numerical integration in the Laplace transform domain by the residue method, as follows

$$f(z) = \mathcal{L}^{-1}\Big[\tilde{f}(s)\Big] = \frac{1}{2\pi j}\int_{\sigma-j_\infty}^{\sigma+j_\infty}\tilde{f}(s)e^{sz}ds = \sum_n \mathrm{Res}\Big[e^{sz}\tilde{f}(s);S_n\Big]. \tag{19}$$

By using the inverse Laplace transform (19), we can compute the output transverse components in the real plane and the output power density at each point at z. The integration path in the right side of the Laplace transform domain includes all the singularities according to Eq. (19). All the points S_n are the poles of $\tilde{f}(s)$ and $\mathrm{Res}[e^{sz}\tilde{f}(s);S_n]$ represent the residue of the function in a specific pole. According to the residue method, two dominant poles for the straight hollow waveguide are given by $s = \pm j\ k(r)$. All the transverse components are known, and the z component of the average-power density Poynting vector is given by

$$S_{av} = \frac{1}{2}\mathrm{Re}\left\{E_r H_\theta{}^* - E_\theta H_r{}^*\right\}, \tag{20}$$

where the asterisk indicates the complex conjugate. The total average-power transmitted along the guide in the z direction can now be

obtained by the integral of Eq. (20) over the waveguide cross section. Thus, the output power transmission is given by

$$T = \frac{1}{2}\int_0^{2\pi}\int_0^a \mathrm{Re}\left\{E_r H_\theta{}^* - E_\theta H_r{}^*\right\} r dr d\theta. \tag{21}$$

In a linear lossy medium, the solution is obtained by replacing the permittivity ϵ by $\epsilon_c = \epsilon - j(\sigma/\omega)$ in the preceding mathematical expressions, where ϵ_c is the complex dielectric constant and σ is the conductivity of the medium. The coefficients are obtained directly from the algebraic Eqs. (11a)–(11d) and are expressed as functions in the Laplace transform domain. To satisfy the metallic boundary conditions of a circular cross-section we find the new roots $P_{1m}^{(new)}$ and $P_{1m}^{'(new)}$ of the equations $J_1(z) = 0$ and $dJ_1(z)/dz = 0$, respectively, where z is complex. The coefficients according to our method are expressed as functions in the Laplace transform domain. Thus, from the requirement that the coefficients vanish, the new roots $P_{1m}^{(new)}$ and $P_{1m}^{'(new)}$ are calculated by developing into the Taylor series, in the first order at $1/\sigma$. Similarly, the roots $P_{1m}^{'(new)}$ are obtained. The new roots in the case of a lossy medium are complex. The complex Bessel functions are computed by using NAG subroutine [19].

It is very interesting to compare between the mode model method for wave propagation in the straight waveguide with a rectangular cross section [20] and this proposed model for the wave propagation in the straight waveguide with a circular cross section. These the two kinds of the different methods enable us to solve practical problems with different boundary conditions. Let us introduce the similar main points. The calculations in all method are based on using Laplace and Fourier transforms, and the output fields are computed by the inverse Laplace and Fourier transforms. Laplace transform on the differential wave equations is needed to obtain the wave equations (and thus also the output fields) that are expressed directly as functions of the transmitted fields at the entrance of the waveguide at $z = 0^+$. Thus, the Laplace transform is necessary to obtain the comfortable and simple *input-output* connections of the fields.

Several examples computed on a Unix system are presented in the next section, in order to demonstrate the results of this proposed method for practical cases with inhomogeneous cross-section in the cylindrical hollow waveguide.

3. NUMERICAL RESULTS

Several examples that demonstrate features of the proposed mode model derived in the previous section. The cross-section of the straight hollow waveguide (Fig. 1) is made of a tube of various types of material, a metallic layer, and a dielectric layer upon it. The next examples represent the case of the hollow waveguide with a metallic layer (Ag) coated by a thin dielectric layer (AgI). For silver having a conductivity of $6.14 \times 10^7 (\text{ohm} \cdot \text{m})^{-1}$ and the skin depth at $10.6\,\mu\text{m}$ is $1.207 \times 10^{-8}\,\text{m}$.

We suppose that the transmitted fields of the initial fields (TEM_{00} mode in excitation) are formulated by using the Fresnel coefficients [Eqs. (16a)–(16d)]. The output modal profile is greatly affected by the parameters of the spot size and the dimensions of the cross section of the waveguide. The geometrical shape of the dielectric profile in the cross section of the cylindrical waveguide is demonstrated in Fig. 1 for an inhomogeneous dielectric profile in the cross section.

In order to solve discontinuous problems in the cross section, the ω_ε function, "cap-shaped function" [21], is used. The ω_ε function (Fig. 3(a)) is defined as

$$\omega_\varepsilon(r) = \begin{cases} C_\varepsilon \exp\left[-\frac{\varepsilon^2}{\varepsilon^2 - |r|^2}\right] & |r| \le \varepsilon \\ 0 & |r| > \varepsilon \end{cases},$$

where the constant C_ε is chosen to satisfy $\int \omega_\varepsilon(r)dr = 1$.

The ω_ε function in the limit $\varepsilon \longrightarrow 0$ is shown in Fig. 3(b). The refractive indices of the air, dielectric and metallic layers are: $n_{(0)} = 1$, $n_{(\text{AgI})} = 2$, and $n_{(\text{Ag})} = 10 - j60$, respectively. The value of the

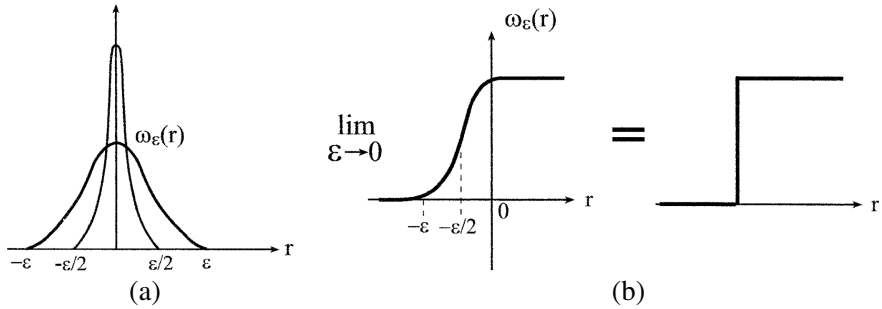

Figure 3. (a) The ω_ε function; (b) The ω_ε function in the limit $\varepsilon \longrightarrow 0$.

refractive index of the material at a wavelength of $\lambda = 10.6\,\mu$m is taken from the table performed by Miyagi et al. [22]. The real and imaginary parts of the refractive indices of the air, dielectric layer (AgI) and metallic layer (Ag) are shown in Fig. 4. Note that the refractive index ($n(r)$) and the transverse derivative of the dielectric profile ($g_r(r)$) are dependent also on the transition's regions in the cross section between the two different materials (air-AgI, AgI-Ag).

The refractive index is calculated as follows

$$n(r)=\begin{cases} n_0 & 0 \le r < b-\varepsilon_1/2 \\ n_0+(n_d-n_0)\exp\left[1-\frac{{\varepsilon_1}^2}{{\varepsilon_1}^2-[r-(b+\varepsilon_1/2)]^2}\right] & b-\varepsilon_1/2 \le r < b+\varepsilon_1/2 \\ n_d & b+\varepsilon_1/2 \le r < a-\varepsilon_2/2 \\ n_d+(n_m-n_d)\exp\left[1-\frac{{\varepsilon_2}^2}{{\varepsilon_2}^2-[r-(a+\varepsilon_2/2)]^2}\right] & a-\varepsilon_2/2 \le r < a+\varepsilon_2/2 \\ n_m & \text{else} \end{cases},$$

where the internal and external diameters are denoted as $2b$, $2a$, and $2(a+\delta_m)$ respectively, where δ_m is the metallic layer. The thickness of the dielectric layer (d) is defined as $[a-b]$, and the thickness of the metallic layer (δ_m) is defined as $[(a+\delta_m)-a]$. The parameters ε_1 and ε_2 are very small [e.g., $\varepsilon_1 = [a-b]/50, \varepsilon_2 = [(a+\delta_m)-a]/50$]. The refractive indices of the air, dielectric and metallic layers are denoted as n_0, n_d, and n_m, respectively. The transverse derivative of the dielectric

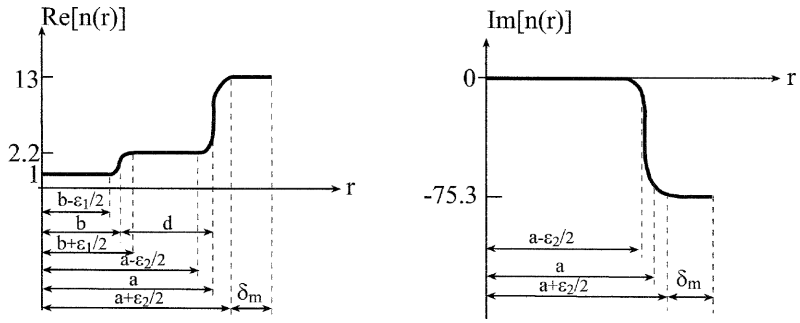

Figure 4. The real and imaginary parts of the refractive indices of the air, dielectric layer (AgI) and metallic layer (Ag).

profile is calculated as follows

$$g_r(r) = \begin{cases} 0 & 0 \le r < b - \varepsilon_1/2 \\ \dfrac{-4(n_d - n_0)\exp\left[1 - \frac{{\varepsilon_1}^2}{{\varepsilon_1}^2 - [r-(b+\varepsilon_1/2)]^2}\right]\left[r-(b+\varepsilon_1/2)\right]{\varepsilon_1}^2}{n_0 + (n_d - n_0)\exp\left[1 - \frac{{\varepsilon_1}^2}{{\varepsilon_1}^2 - [r-(b+\varepsilon_1/2)]^2}\right]\left[{\varepsilon_1}^2 - [r-(b+\varepsilon_1/2)]^2\right]^2} & b - \varepsilon_1/2 \le r < b + \varepsilon_1/2 \\ 0 & b + \varepsilon_1/2 \le r < a - \varepsilon_2/2 \\ \dfrac{-4(n_m - n_d)\exp\left[1 - \frac{{\varepsilon_2}^2}{{\varepsilon_2}^2 - [r-(a+\varepsilon_2/2)]^2}\right]\left[r-(a+\varepsilon_2/2)\right]{\varepsilon_2}^2}{n_d + (n_m - n_d)\exp\left[1 - \frac{{\varepsilon_2}^2}{{\varepsilon_2}^2 - [r-(a+\varepsilon_2/2)]^2}\right]\left[{\varepsilon_2}^2 - [r-(a+\varepsilon_2/2)]^2\right]^2} & a - \varepsilon_2/2 \le r < a + \varepsilon_2/2 \\ 0 & \text{else} \end{cases} .$$

Figure 4 shows the real and imaginary parts of the refractive indices of the air, dielectric layer (AgI) and metallic layer (Ag), for the cross-section of the straight hollow waveguide, as shown in Fig. 1.

In algebraic Eqs. (11a)–(11d), we assumed $n' = n = 1$. The convergence of the numerical results were obtained for $n' = n = 1$, where $m' = 1, \ldots, N$, and where $N = 20$.

The results of the output transverse components of the fields and the output power density ($|S_{av}|$) (e.g., Fig. 5(a)) show the behavior of the solutions for the TEM_{00} mode in excitation. The result of the output power density (S_{av}) of this example (Fig. 5(a)) is compared to the result of the published experimental data [23], as shown also in

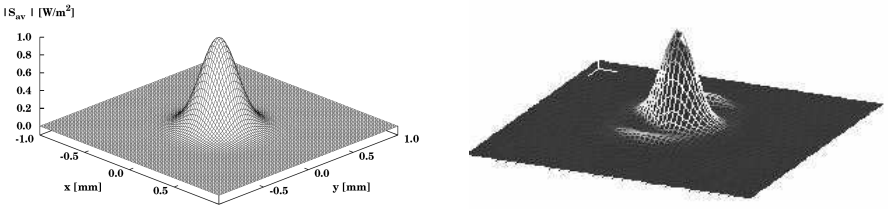

(a) (b)

Figure 5. The output power density ($a = 1\,\text{mm}$, $d_{(\text{AgI})} = 0.75\,\mu\text{m}$, $\lambda = 10.6\,\mu\text{m}$, $w_0 = 0.3\,\text{mm}$, $n_{(0)} = 1$, $n_{(\text{AgI})} = 2.2$, $n_{(\text{Ag})} = 13.5 - j75.3$, and the length of the straight waveguide is 1 m) (a) theoretical result; (b) Experimental result.

Fig. 5(b). This comparison has shown good agreement (a Gaussian shape) as expected, except for the secondary small propagation mode. In this example, the length of the straight waveguide is 1 m, the diameter ($2a$) of the waveguide is 2 mm, the thickness of the dielectric layer [$d_{(\mathrm{AgI})}$] is 0.75 µm, and the minimum spot-size (w_0) is 0.3 mm. The refractive indices of the air, dielectric layer (AgI) and metallic layer (Ag) are $n_{(0)} = 1$, $n_{(\mathrm{AgI})} = 2.2$, and $n_{(\mathrm{Ag})} = 13.5 - j75.3$, respectively. The value of the refractive index of the material at a wavelength of $\lambda = 10.6\,\mu\mathrm{m}$ is taken from the table performed by Miyagi, et al. [22]. This experimental result was obtained from the measurements of the

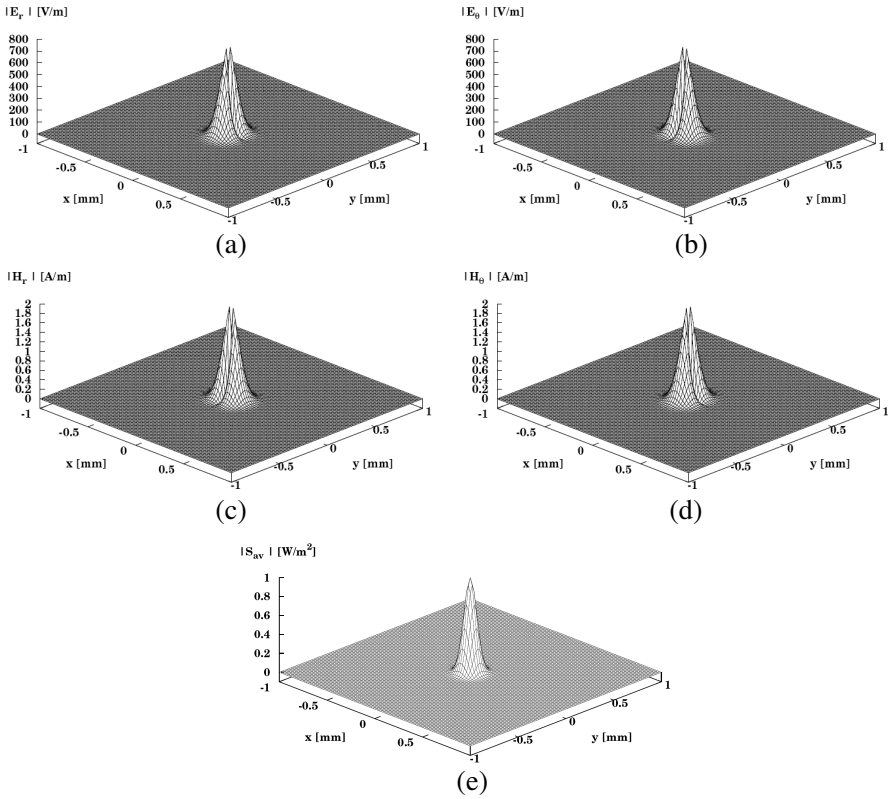

Figure 6. The results of the output transverse components of the field where $w_0 = 0.1\,\mathrm{mm}$, and $a = 1\,\mathrm{mm}$ (a) E_r component; (b) E_θ component; (c) H_r component; (d) H_θ component; (e) The result of the output power density, where $z = 1\,\mathrm{m}$, $n_d = 2.2$, and $n_{(\mathrm{Ag})} = 13.5 - j75.3$.

transmitted CO_2 laser radiation ($\lambda = 10.6\,\mu m$) propagation through a hollow tube covered on the bore wall with silver and silver-iodide layers (Fig. 1). The experimental result (Fig. 5(b)) is affected by the additional parameters (e.g., the roughness of the internal wall of the waveguide) which are not taken theoretically into account.

The two important parameters that we studied were the spot size and the dimensions of the cross section of the straight hollow waveguide. The results are affected by the spot size and the dimensions of the cross section of the waveguide. The waveguide's cross-section consists of the metallic and dielectric coating (Fig. 1). The results of the output transverse components of the field are shown in Figs. 6(a)–

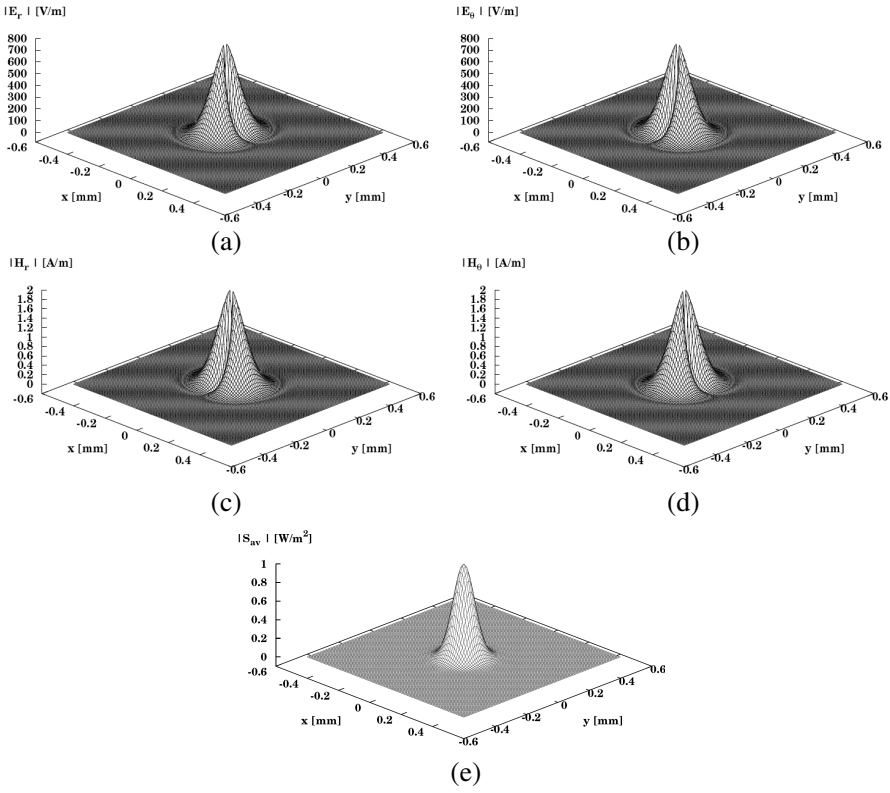

Figure 7. The results of the output transverse components of the field where $w_0 = 0.1\,\text{mm}$, and $a = 0.5\,\text{mm}$ (a) E_r component; (b) E_θ component; (c) H_r component; (d) H_θ component; (e) The result of the output power density, where $z = 1\,\text{m}$, $n_d = 2.2$, and $n_{(\text{Ag})} = 13.5 - j75.3$.

6(d), and the result of the output power density is shown in Fig. 6(e), where $w_0 = 0.1\,\text{mm}$, $a = 1\,\text{mm}$, $z = 1\,\text{m}$, $n_{(0)} = 1$, $n_{(\text{AgI})} = 2.2$, and $n_{(\text{Ag})} = 13.5 - j75.3$.

By changing only the parameter $a = 1\,\text{mm}$ to $a = 0.5\,\text{mm}$, where the other parameters are not changed, the results of the output transverse components are demonstrated in Figs. 7(a)–7(d) and the output power density is demonstrated in Fig. 7(e). By changing only the parameter $w_0 = 0.1\,\text{mm}$ to $w_0 = 0.25\,\text{mm}$, where the other parameters are not changed, the results of the output transverse components are shown in Figs. 8(a)–8(d), and the output power density is shown in Fig. 8(e). In addition to the main propagation mode,

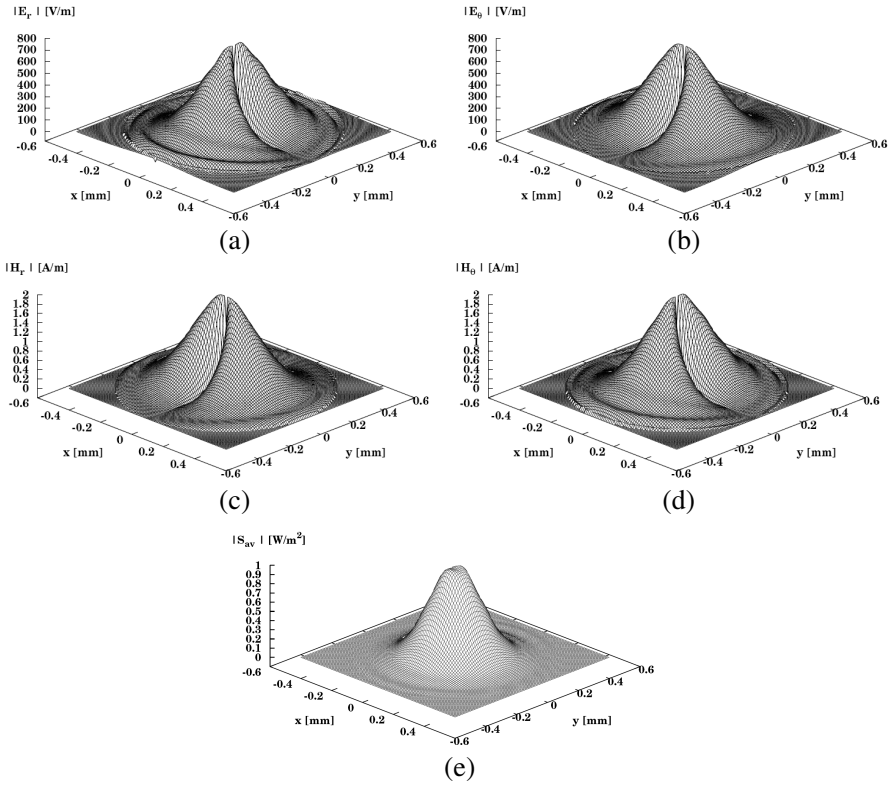

Figure 8. The results of the output transverse components of the field where $w_0 = 0.25\,\text{mm}$, and $a = 0.5\,\text{mm}$ (a) E_r component; (b) E_θ component; (c) H_r component; (d) H_θ component ; (e) The result of the output power density, where $z = 1\,\text{m}$, $n_d = 2.2$, and $n_{(\text{Ag})} = 13.5 - j75.3$.

several other secondary modes and symmetric output shape appear in Figs. 8(a)–8(e) for $a = 0.5\,\text{mm}$ and $w_0 = 0.25\,\text{mm}$.

Figures 9(a)–9(c) show the results of the output power density where $a = 0.5\,\text{mm}$ in three cases of the spot size $w_0 = 0.15\,\text{mm}$, $w_0 = 0.2\,\text{mm}$, and $w_0 = 0.25\,\text{mm}$, respectively. The other parametrs are $z = 1\,\text{m}$, $n_d = 2.2$, and $n_{(\text{Ag})} = 13.5 - j75.3$. Fig. 9(d) shows the result of the output power density of the central peak in the same cross section of the three cases, where $y = b/2$, for $w_0 = 0.15\,\text{mm}$, $w_0 = 0.2\,\text{mm}$, and $w_0 = 0.25\,\text{mm}$, respectively.

By changing only the three values of the spot size from $w_0 = 0.15\,\text{mm}$, $w_0 = 0.2\,\text{mm}$, and $w_0 = 0.25\,\text{mm}$, to $w_0 = 0.26\,\text{mm}$, $w_0 = 0.28\,\text{mm}$, and $w_0 = 0.3\,\text{mm}$, respectively, the results of the output power density for $a = 0.5\,\text{mm}$ are demonstrated in Figs. 10(a)–10(c). Fig. 10(d) shows the result of the output power density of the central peak in the same cross section of the three cases, where $y = b/2$, for $w_0 = 0.26\,\text{mm}$, $w_0 = 0.28\,\text{mm}$, and $w_0 = 0.3\,\text{mm}$, respectively. The output modal profile is greatly affected by the parameters of the

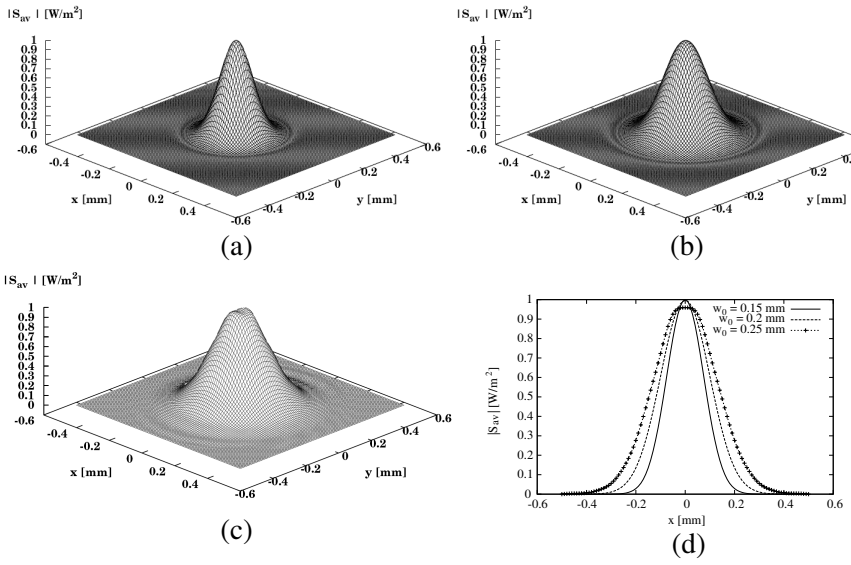

Figure 9. The output power density where $a = 0.5\,\text{mm}$ in three cases: (a) $w_0 = 0.15\,\text{mm}$; (b) $w_0 = 0.2\,\text{mm}$; (c) $w_0 = 0.25\,\text{mm}$. The other parametrs are $z = 1\,\text{m}$, $n_d = 2.2$, and $n_{(\text{Ag})} = 13.5 - j75.3$; (d) The output power density of the central peak in the same cross section of the three cases (a)–(c), where $y = b/2$, for $w_0 = 0.15\,\text{mm}$, $w_0 = 0.2\,\text{mm}$, and $w_0 = 0.25\,\text{mm}$, respectively.

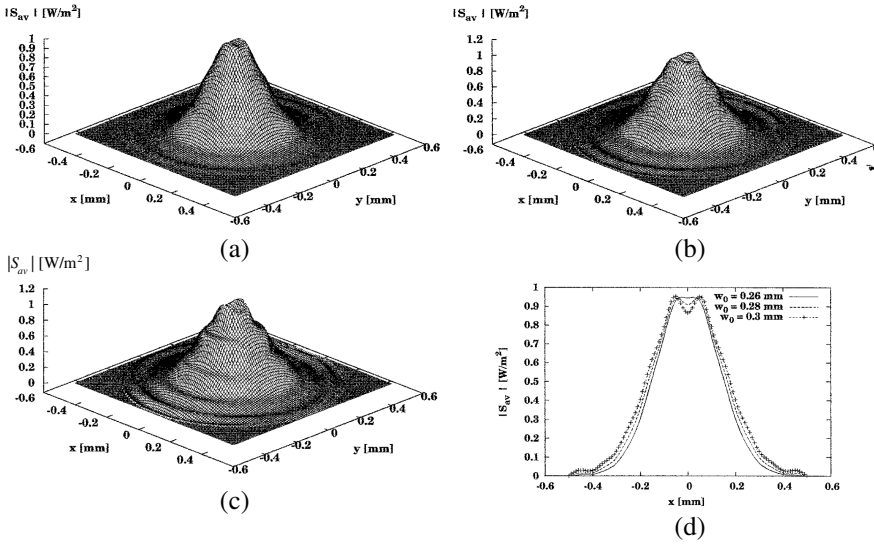

Figure 10. The output power density where $a = 0.5\,\text{mm}$ in three cases: (a) $w_0 = 0.26\,\text{mm}$; (b) $w_0 = 0.28\,\text{mm}$; (c) $w_0 = 0.3\,\text{mm}$. The other parametrs are $z = 1\,\text{m}$, $n_d = 2.2$, and $n_{(\text{Ag})} = 13.5 - j75.3$; (d) The output power density of the central peak in the same cross section of the three cases (a)–(c), where $y = b/2$, for $w_0 = 0.26\,\text{mm}$, $w_0 = 0.28\,\text{mm}$, and $w_0 = 0.3\,\text{mm}$, respectively.

spot size and the dimensions of the cross section of the waveguide. Figs. 10(a)–10(c) demonstrate that in addition to the main propagation mode, several other secondary modes and symmetric output shape appear in the results of the output power density for the three values of $w_0 = 0.26\,\text{mm}$, $w_0 = 0.28\,\text{mm}$, and $w_0 = 0.3\,\text{mm}$, respectively.

4. CONCLUSIONS

This paper presents a rigorous approach for the propagation of EM fields along a cylindrical hollow waveguide. The main objective was to develop a numerical method for the calculation of the output fields and power density in the case of the straight and the hollow waveguide. The other objectives were to present the technique to calculate the dielectric profiles and their transverse derivatives in the inhomogeneous cross section of the straight hollow waveguide, and to understand the influence of the spot-size and cross section on the output fields and output power density. The derivation is based on Maxwell's equations.

The longitudinal components of the fields were developed into the Fourier-Bessel series. The transverse components of the fields were expressed as functions of the longitudinal components in the Laplace plane and were obtained by using the inverse Laplace transform by the residue method. The separation of variables was obtained by using the orthogonal-relations. These objectives contribute to the application of the model for the straight hollow waveguide.

The results of the output transverse components of the fields and the output power density ($|S_{av}|$) (e.g., Fig. 5(a)) show the behavior of the solutions for the TEM_{00} mode in excitation. The comparison between the theoretical mode-model (Fig. 5(a)) and the experimental data (Fig. 5(b)) has shown good agreement (a Gaussian shape) as expected, except for the secondary small propagation mode. This experimental result was obtained from the measurements of the transmitted CO_2 laser radiation ($\lambda = 10.6\,\mu\text{m}$) propagation through a hollow tube covered on the bore wall with silver and silver-iodide layers (Fig. 1). The experimental result (Fig. 5(b)) is affected by the additional parameters (e.g., the roughness of the internal wall of the waveguide) which are not taken theoretically into account.

By changing only the parameter $a = 1\,\text{mm}$ to $a = 0.5\,\text{mm}$, where the other parameters are not changed, the results of the output transverse components are demonstrated in Figs. 7(a)–7(d) and the output power density is demonstrated in Fig. 7(e). By changing only the parameter $w_0 = 0.1\,\text{mm}$ to $w_0 = 0.25\,\text{mm}$, where the other parameters are not changed, the results of the output transverse components are shown in Figs. 8(a)–8(d), and the output power density is shown in Fig. 8(e).

By changing only the three values of the spot size to $w_0 = 0.26\,\text{mm}$, $w_0 = 0.28\,\text{mm}$, and $w_0 = 0.3\,\text{mm}$, respectively, the results of the output power density of the field for $a = 0.5\,\text{mm}$ are demonstrated in Figs. 10(a)–10(c). Fig. 10(d) shows the result of the output power density of the central peak in the same cross section of the three cases, where $y = b/2$, for $w_0 = 0.26\,\text{mm}$, $w_0 = 0.28\,\text{mm}$, and $w_0 = 0.3\,\text{mm}$, respectively.

The two important parameters that we studied were the spot size and the dimensions of the cross section of the straight hollow waveguide. The output results are affected by the parameters of the spot size and the dimensions of the cross section of the waveguide. In addition to the main propagation mode, several other secondary modes and symmetric output shape appear in Figs. 8(a)–8(d) for $a = 0.5\,\text{mm}$ and $w_0 = 0.25\,\text{mm}$. Figs. 10(a)–10(c) demonstrate that in addition to the main propagation mode, several other secondary modes and symmetric output shape appear in the results of the output power

density for the three values of $w_0 = 0.26\,\text{mm}$, $w_0 = 0.28\,\text{mm}$, and $w_0 = 0.3\,\text{mm}$, respectively.

APPENDIX A.

The elements of the matrices ($G_{00}^{(1)mm'}$, etc.) are given by:

$$G_{00}^{(1)mm'} = \int_0^a J_1\left(P_{1m'}\frac{r}{a}\right) J_1\left(P_{1m}\frac{r}{a}\right) r dr \delta_{1n},$$

$$G_{01}^{(1)mm'} = \int_0^a g(r) J_1\left(P_{1m'}\frac{r}{a}\right) J_1\left(P_{1m}\frac{r}{a}\right) r dr \delta_{1n},$$

$$G_{02}^{(1)mm'} = \int_0^a k^2 g(r) J_1\left(P_{1m'}\frac{r}{a}\right) J_1\left(P_{1m}\frac{r}{a}\right) r dr \delta_{1n},$$

$$G_{03}^{(1)mm'} = \int_0^a g_r\left(\frac{P_{1m'}}{a}\right) J_1{}'\left(P_{1m'}\frac{r}{a}\right) J_1\left(P_{1m}\frac{r}{a}\right) r dr,$$

$$G_{04}^{(1)mm'} = \int_0^a g_r J_1{}'\left(\frac{p'_{1m'}r}{a}\right) J_1\left(P_{1m}\frac{r}{a}\right) dr \delta_{1n}.$$

Similarly, the remaining elements are obtained. The coefficients are obtained directly from the algebraic system of Eqs. (11a)–(11d) and are expressed as functions in s-plane.

REFERENCES

1. Harrington, J. A. and Y. Matsuura, "Review of hollow waveguide technology," *Proc. SPIE*, Vol. 2396, 4–14, 1995.
2. Harrington, J. A., D. M. Harris, and A. Katzir, *Biomedical Optoelectronic Instrumentation*, 4–14, 1995.
3. Harrington, J. A., "A review of IR transmitting, hollow waveguides," *Fiber and Integrated Optics*, Vol. 19, 211–228, 2000.
4. Marhic, M. E., "Mode-coupling analysis of bending losses in IR metallic waveguides," *Appl. Opt.*, Vol. 20, 3436–3441, 1981.
5. Croitoru, N., E. Goldenberg, D. Mendlovic, S. Ruschin, and N. Shamir, "Infrared chalcogenide tube waveguides," *Proc. SPIE*, Vol. 618, 140–145, 1986.
6. Novotny, L. and C. Hafner, "Light propagation in a cylindrical waveguide with a complex, metallc, dielectric function," *Physical Review E*, Vol. 50, 4094–4106, 1994.

7. Yener, N., "Advancement of algebraic function approximation in eigenvalue problems of lossless metallic waveguides to infinite dimensions, Part I: Properties of the operator in infinite dimensions," *Journal of Electromagnetic Waves and Applications*, Vol. 20, No. 12, 1611–1628, 2006.
8. Yener, N., "Algebraic function approximation in eigenvalue problems of lossless metallic waveguides: Examples," *Journal of Electromagnetic Waves and Applications*, Vol. 20, No. 6, 731–745, 2006.
9. Khalaj-Amirhosseini, M., "Analysis of longitudinally inhomogeneous waveguides using Taylor's series expansion," *Journal of Electromagnetic Waves and Applications*, Vol. 20, No. 8, 1093–1100, 2006.
10. Khalaj-Amirhosseini, M., "Analysis of longitudinally inhomogeneous waveguides using the Fourier series expansion," *Journal of Electromagnetic Waves and Applications*, Vol. 20, No. 10, 1299–1310, 2006.
11. Reutskiy, S. Y., "The methods of external excitation for analysis of arbitrarily-shaped hollow conducting waveguides," *Progress In Electromagnetics Research*, Vol. 82, 203–226, 2008.
12. Jackson, J. D., *Classical Electrodynamics*, 3rd Edition, John Wiley and Sons, 1999.
13. Hildebrand, F. B., *Advanced Calculus for Applications*, 2nd Edition, Prentice Hall Inc., 1976.
14. Collin, R. E., *Foundation for Microwave Engineering*, McGraw-Hill, New York, 1996.
15. Yariv, A., *Optical Electronics*, 3rd Edition, Holt-Saunders Int. Editions, 1985.
16. Baden Fuller, A. J., *Microwaves*, Chap. 5, 118–120, Pergamon Press, A. Wheaton and Co. Ltd, Oxford, 1969.
17. Olver, F. W. J., *Royal Society Mathematical Tables, Zeros and Associated Values*, 2–30, University Press Cambridge, 1960.
18. Jahnke, E. and F. Emde, *Tables of Functions with Formulae and Curves*, Chap. 8, 166, Dover Publications, New York, 1945.
19. The Numerical Algorithms Group (NAG) Ltd., Wilkinson House, Oxford, U.K..
20. Menachem, Z. and E. Jerby, "Transfer matrix function (TMF) for wave propagation in dielectric waveguides with arbitrary transverse profiles," *IEEE Trans. Microwave Theory Tech.*, Vol. 46, 975–982, 1998.
21. Vladimirov, V., *Equations of Mathematical Physics*, 1971.

22. Miyagi, M., K. Harada, and S. Kawakami, "Wave propagation and attenuation in the general class of circular hollow waveguides with uniform curvature," *IEEE Trans. Microwave Theory Tech.*, Vol. 32, 513–521, 1984.
23. Croitoru, N., A. Inberg, M. Oksman, and M. Ben-David, "Hollow silica, metal and plastic waveguides for hard tissue medical applications," *Proc. SPIE*, Vol. 2977, 30–35, 1997.